Supporting information

Exploring Stacking Pressure-Induced Mechanical Failure of Ni-Rich Cathode in Sulfide Solid-State Batteries

Yiman Feng, [a] Zhixing Wang, [a] Gui Luo, [b] Duo Deng, [b] Wenjie Peng, [a,b] Wenchao Zhang, [a] Hui Duan, [a] Feixiang Wu, [a,c] Xing Ou, [a] Junchao Zheng, [a,c] and Jiexi Wang [a,c,*]

[a] National Energy Metal Resources and New Materials Key Laboratory, Engineering Research Center of the Ministry of Education for Advanced Battery Materials, Hunan Provincial Key Laboratory of Nonferrous Value-Added Metallurgy, School of Metallurgy and Environment, Central South University, Changsha 410083, China

[b] BASF Shanshan Battery Materials Co LTD, Changsha 410205, China

[c] National Engineering Research Centre of Advanced Energy Storage Materials, Changsha 410205, China

Corresponding Author

* Corresponding author, Email address: wangjiexikeen@csu.edu.cn

EXPERIMENTAL SECTION

Materials

As shown in Figure S1, the $LiNi_{0.95}Co_{0.04}Mn_{0.01}O_2$ (NCM95, BASF Shanshan Battery Materials Co. LTD) exhibits well-defined single-crystal morphology with a relatively uniform particle size distribution (2–3 μm).

Material characterization

The surface morphology of the materials was characterized using a field-emission scanning electron microscope (SEM, JSM-7610FPlus, JEOL) and electron backscattered diffraction (EBSD) mode. The accelerating voltage was set to 5.0 kV, and the working distance was approximately 8.0 mm, with specific values adjustable according to the actual conditions of the samples. The microstructural features were evaluated using high-resolution transmission electron microscopy (HRTEM, Titan G2 60-300). The crystal structure of the samples was analyzed with an X-ray diffractometer (XRD, MiniFlex600, Rigaku) operating at a current of 40 mA and a voltage of 40 kV, with Cu-Kα radiation (λ = 0.154 nm). CalAtom was used to simulate the HRTEM images, revealing details of the material's atomic arrangement, crystal defects (such as dislocations and vacancies), and interface structures. The intensity of each atomic column was estimated based on the intensity distribution obtained through the maximum entropy filtering (MEF) method. The elemental composition and chemical state of the samples were determined using X-ray photoelectron spectroscopy (XPS) with a PHI Versa Probe 4 instrument. The C 1s spectrum at 284.8 eV was used as the reference for spectral calibration. Raman spectra were collected using a Thermo Scientific DXR3xi Raman spectrometer with a

laser wavelength of 532 nm, and the Raman spectral intensity values were recorded in the range of 100–3000 cm^{-1}. Electron paramagnetic resonance (EPR) measurements for oxygen vacancies were performed using a Bruker E500 spectrometer. The experiments were performed at room temperature (RT) with an X-band microwave frequency of 9.8 GHz. The modulation frequency was set to 100 kHz, with a modulation amplitude of 0.1 mT and a microwave power of 2 mW. The magnetic field was scanned over a range from 330 to 350 mT. The resulting EPR spectra were analyzed to identify the g-values characteristic of oxygen vacancies. Additionally, the peak intensity was quantified to facilitate comparison across different samples. To prevent exposure to air, all the aforementioned samples were prepared in a high-purity argon-filled glovebox, and tested under anhydrous and oxygen-free conditions.

To characterize the pore structure of the electrode, a nano-computed tomography system (CT, Phoenix v|tome|x s, General Electric, USA) was employed. The operating voltage of the X-ray source in this system was 180 kV, the power was 15 W, and the spatial resolution was set to 500 nm. Avizo software was used for 3D structural rendering to visualize the spatial distribution of pores. The pore and solid phases were segmented by thresholding, and the ratio of pore volume to total sample volume was calculated.

Cell assembly and electrochemical measurement

LiIn sulfide ASSLBs assembly. As shown in **Figure S2**, a composite cathode was prepared by mixing NCM95 and Li_6PS_5Cl (LPSC, Zhejiang FunLithium New Energy Technology Co. LTD) at a weight ratio of 7:3. The mixture was stirred at 300 rpm for 360 seconds using a mechanical

stirrer to ensure homogeneity. A custom mold was used to manufacture the stacked particle cell. Initially, 85 mg of LPSC was evenly distributed within the mold. The battery was then compacted at 125 MPa to consolidate the sulfide SSE. Following this, 10 mg of the cathode composite was applied to the consolidated SSE and compacted again at 375 MPa. To form the LiIn alloy anode, indium and lithium foils were placed sequentially on the anode side of the mold. Finally, stacking pressures ranging from 125 to 375 MPa were applied to the entire battery to investigate the effect of stacking pressure on the mechanical failure of the NRLOs. The batteries were labeled according to the applied pressure as LiIn-pressure (where pressure = 125, 250, 375 MPa).

LTO sulfide ASSLBs assembly. As shown in **Figure S3**, a composite cathode was prepared by mixing NCM95 and LPSC at a weight ratio of 7:3 and a composite anode was prepared by mixing LTO, LPSC, and vinyl graphene carbon fiber (VGCF, canrud) in a weight ratio of 50:50:3. The resulting mixtures were separately stirred at 300 rpm for 360 seconds using a mechanical stirrer to achieve uniformity. A custom mold was employed to fabricate the stacked granular battery. Initially, 22 mg of the composite anode was evenly distributed within the mold and compacted at 375 MPa. Following this, 85 mg of the sulfide SSE was layered onto the compacted composite anode and compacted again at 125 MPa. Subsequently, 6 mg of the composite cathode was placed on top of the sulfide SSE, and the entire assembly was compacted at 375 MPa to ensure tight contact between the solid particles. To investigate the effect of stacking pressure on the mechanical failure of NRLOs, stacking pressures ranging from 125 to 375 MPa were applied. The batteries were labeled according to the applied pressure as LTO-pressure (where pressure = 125, 250, 375). The entire assembly process was

conducted in an argon-filled glove box, maintaining H_2O and O_2 concentrations below 0.01 ppm to ensure an inert environment.

Electrochemical measurement. Galvanostatic charge and discharge tests were conducted at 25 °C using a LAND battery testing system (1C = 190 mA g^{-1}), within a voltage range of 2.7 to 4.3 V vs. Li/Li^+. A four-channel solid-state battery temperature-pressure testing system (CL-001), manufactured by Ningbo Chuangli, was employed to monitor in situ pressure changes during battery charging and discharging at a rate of 0.1C. EIS measurements were performed using a PARSTAT 4000A electrochemical workstation. The test parameters included a frequency spectrum ranging from 10^{-2} to 10^6 Hz and a signal amplitude of 10 mV. In situ EIS measured impedance every 0.1 V. DRT analysis was conducted using EIS data from the sulfide ASSLBs. Valid EIS data were exported and processed using the DRTtools MATLAB toolbox with Tikhonov regularization. The time constant (τ) range was 10^{-6}–10^2 s, and the regularization parameter (λ) was optimized via the L-curve method. DRT curves were analyzed to identify electrochemical processes, with peak parameters extracted for quantification. Sulfide ASSLBs underwent Linear Sweep Voltammetry (LSV) measurements utilizing a Squidstat electrochemical workstation. 85 mg of the sulfide SSE was placed into a mold cell with a 10 mm inner diameter, and a pressure of 125 MPa was applied. Subsequently, an indium foil and a lithium foil were sequentially placed as the counter electrode, and a stacking pressure of 125–370 MPa was applied for the LSV test. The voltage scan rate was set to 0.1 mV per second, and the test temperature was RT.

The Galvanostatic Intermittent Titration Technique (GITT) was performed with a 600 s charge/discharge at 0.1 C followed by 5400 s of relaxation.

In-situ DEMS tests. In-situ gas evolution detection of the battery was performed using a Hiden HPR-40 DEMS (Hiden Analytical), which allowed for the real-time monitoring of the type and quantity of gases produced during the electrochemical process of the battery. Ultra-high-purity helium gas (99.999% pure) was used as the carrier gas during testing. The DEMS was integrated with an electrochemical workstation (SP-150) to facilitate in situ analysis of gas evolution during electrochemical processes at RT. The test voltage range was 2.7 to 4.3 V vs. Li/Li^+, with a charge and discharge rate of 0.1C.

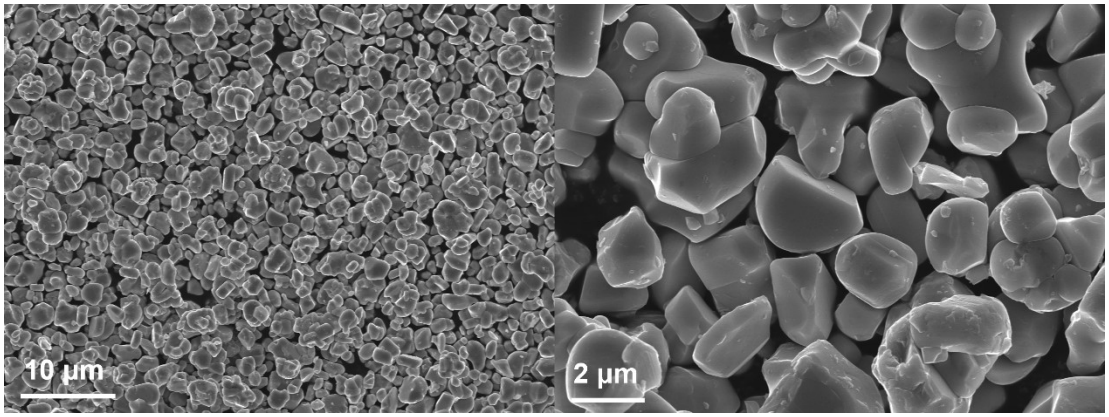

Figure S1. The morphology and size of NCM95.

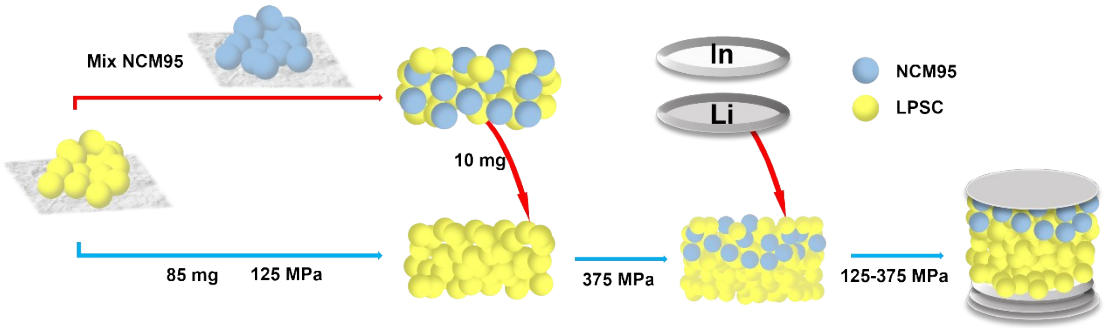

Figure S2. Schematic diagram of LiIn sulfide ASSLB assembly.

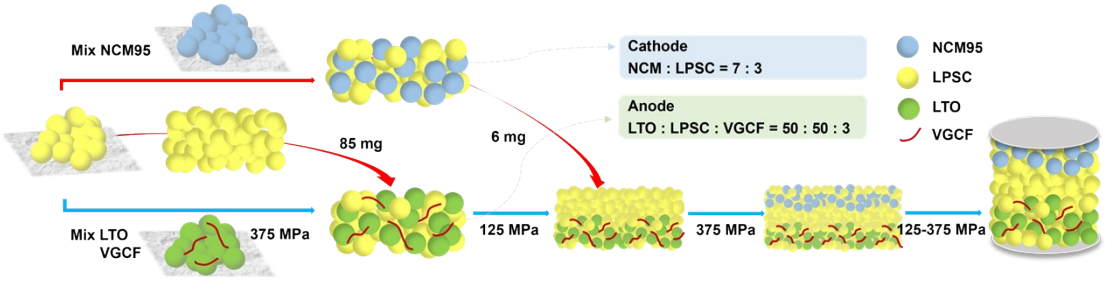

Figure S3. Schematic diagram of LTO sulfide ASSLB assembly.

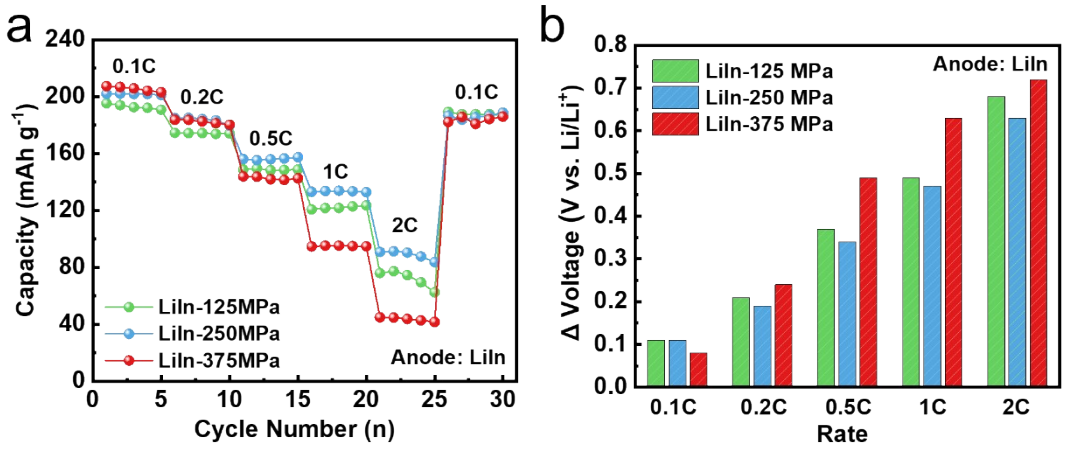

Figure S4. (a) Rate performance of LiIn sulfide ASSLBs ranging from 0.1C to 2C. (b) Discharge voltage drop of LiIn sulfide ASSLBs from 0.1C to 2C.

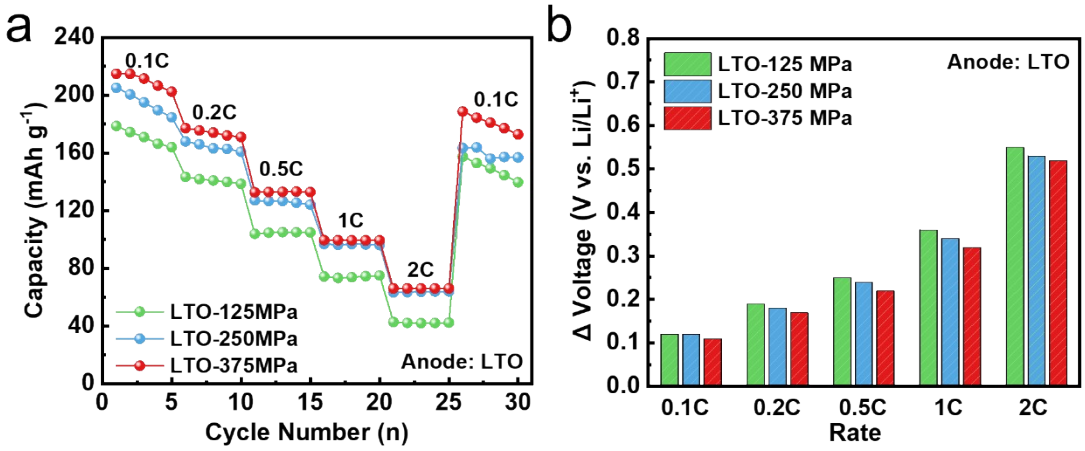

Figure S5. (a) Rate performance of LTO sulfide ASSLBs ranging from 0.1C to 2C. (b) Discharge voltage drop of LTO sulfide ASSLBs from 0.1C to 2C.

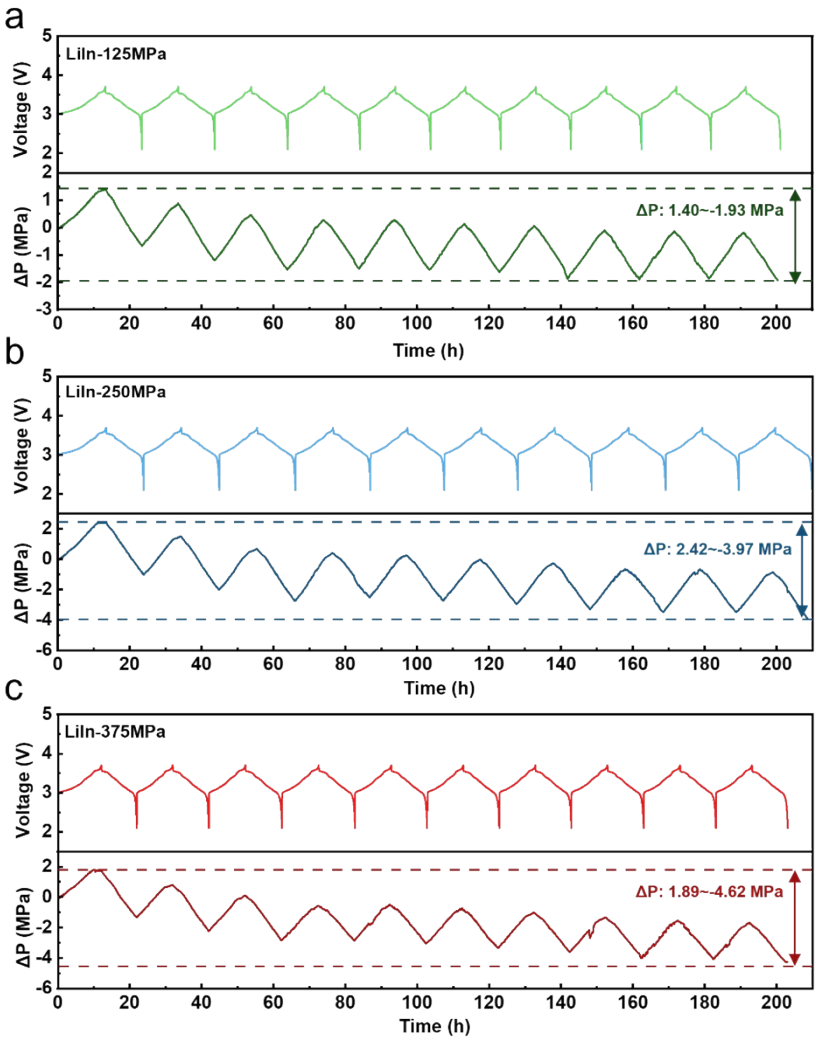

Figure S6. Pressure change during the cycling of (a) LiIn-125MPa, (b) LiIn-250MPa, and (c) LiIn-375MPa.

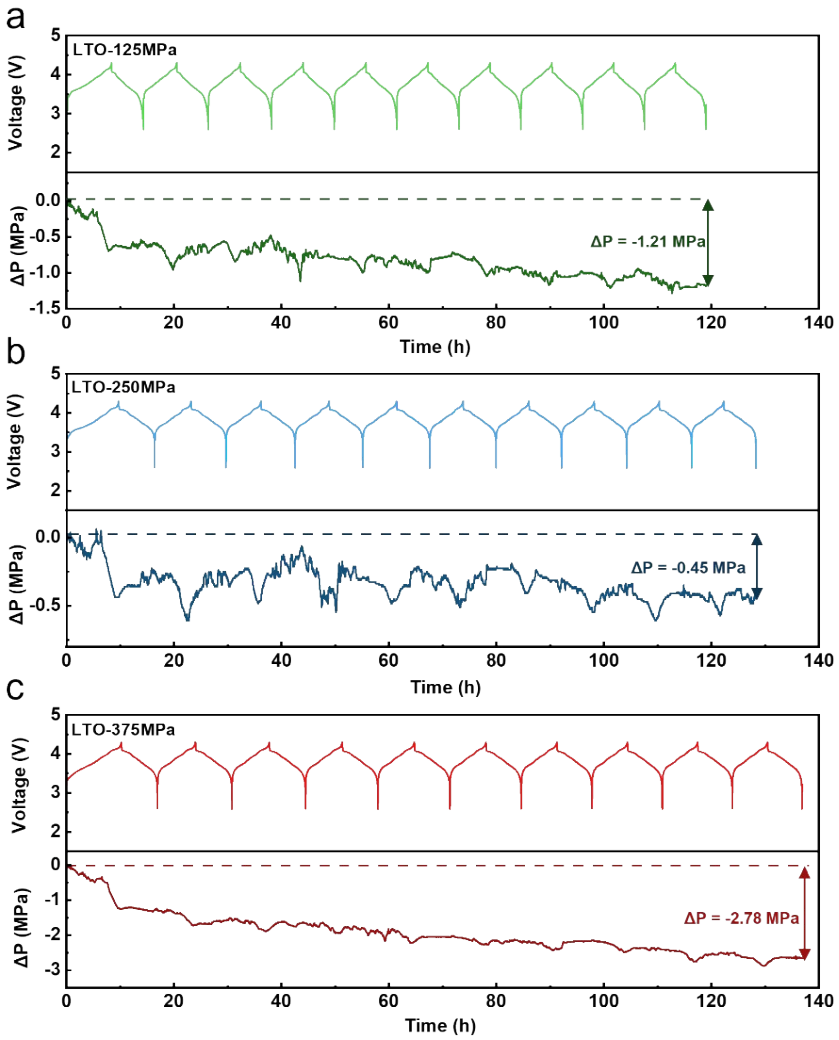

Figure S7. Pressure change during the cycling of (a) LTO-125MPa, (b) LTO-250MPa, and (c) LTO-375MPa.

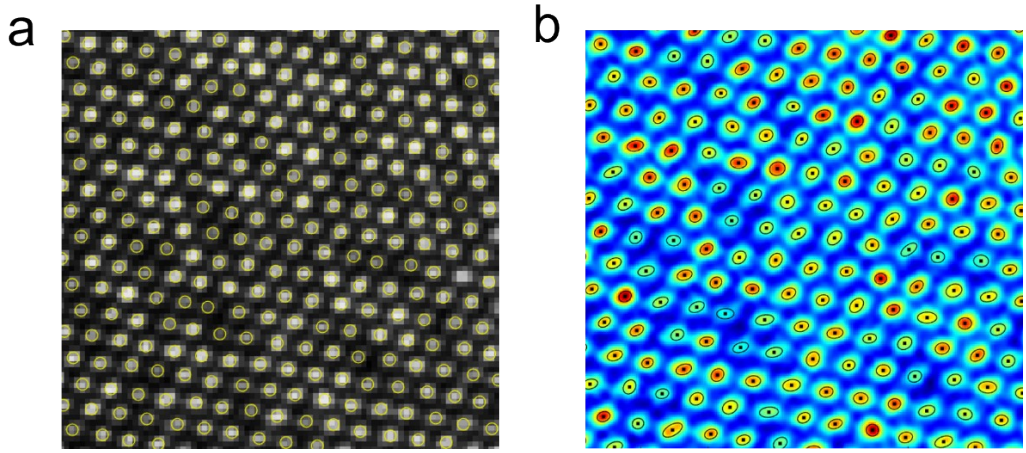

Figure S8. (a-b) HRTEM images and CalAtom simulation result of NCM95 after standing at 250 MPa.

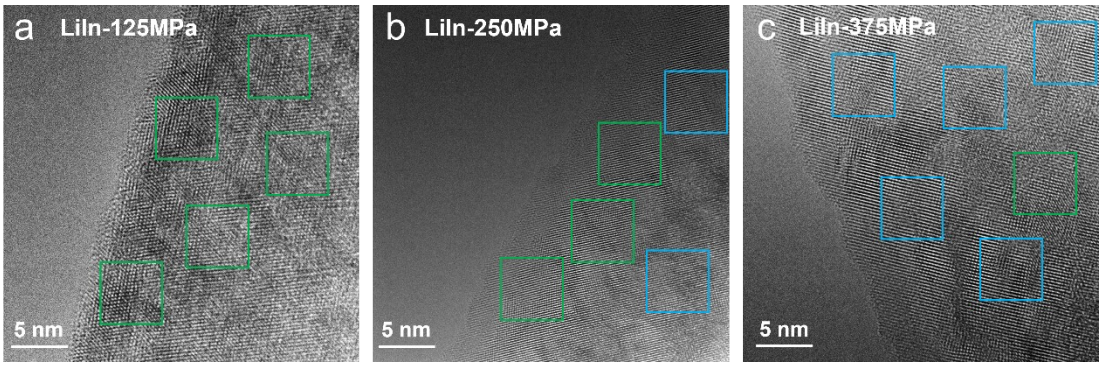

Figure S9. CAM surface version HRTEM of (a) LiIn-125MPa, (b) LiIn-250MPa, and (c) LiIn-375MPa after first charging and discharging.

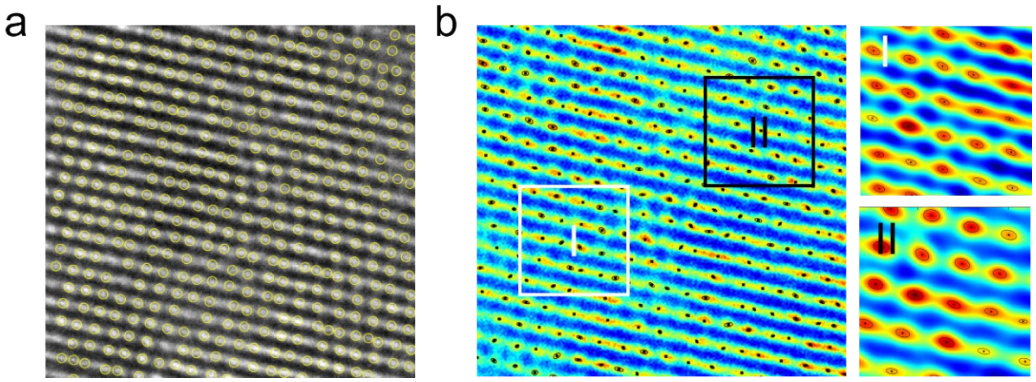

Figure S10. (a-b) HRTEM images and CalAtom simulation result for NCM95 of LiIn-250MPa after first charging and discharging.

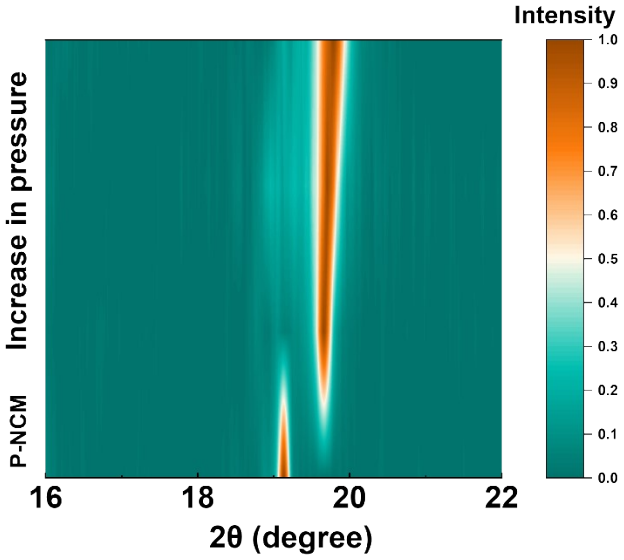

Figure S11. XRD for the composite cathode after first charging and discharging under different stacking pressure.

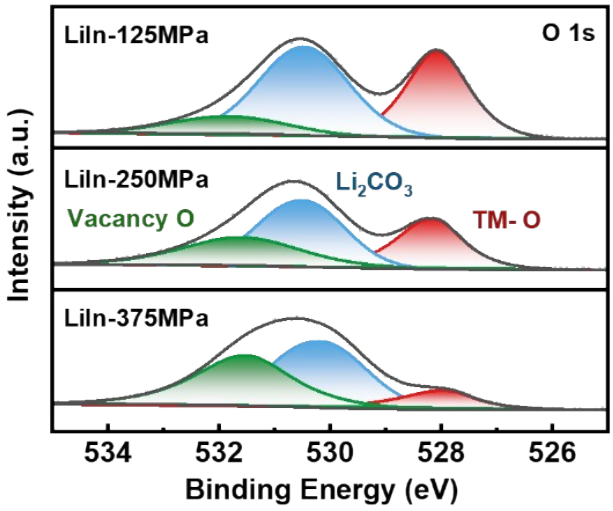

Figure S12. The XPS spectra of O 1s for the composite cathode after first charging and discharging under different stacking pressure.

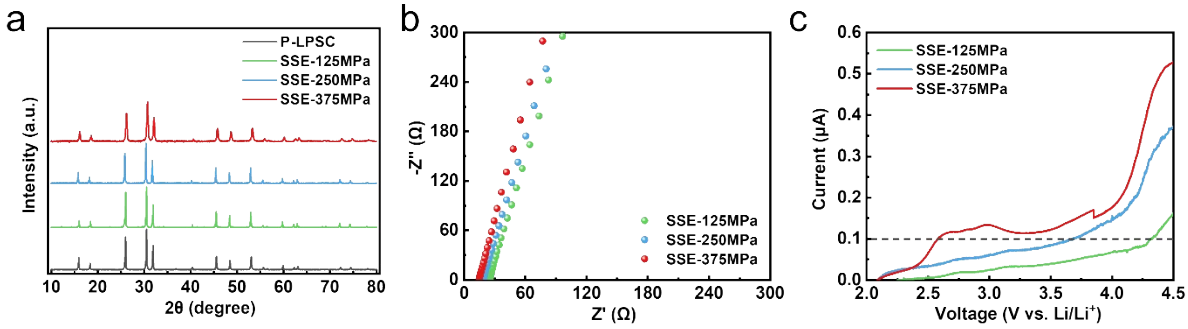

Figure S13. (a)XRD, (b) EIS, and (c)LSV curves of sulfide SSE under different stacking pressures.

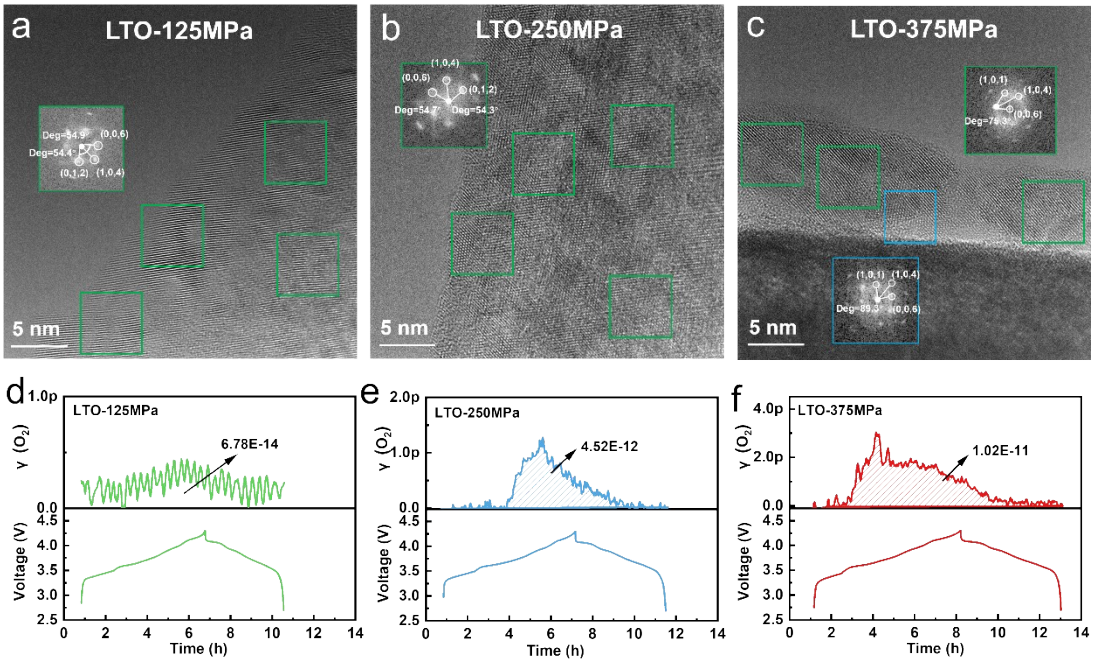

Figure S14. CAM surface version HRTEM of (a) LTO-125MPa, (b) LTO-250MPa, and (c) LTO-375MPa after first charging and discharging. O_2 production of (d) LTO-125MPa, (e) LTO-250MPa, and (f) LTO-375MPa.

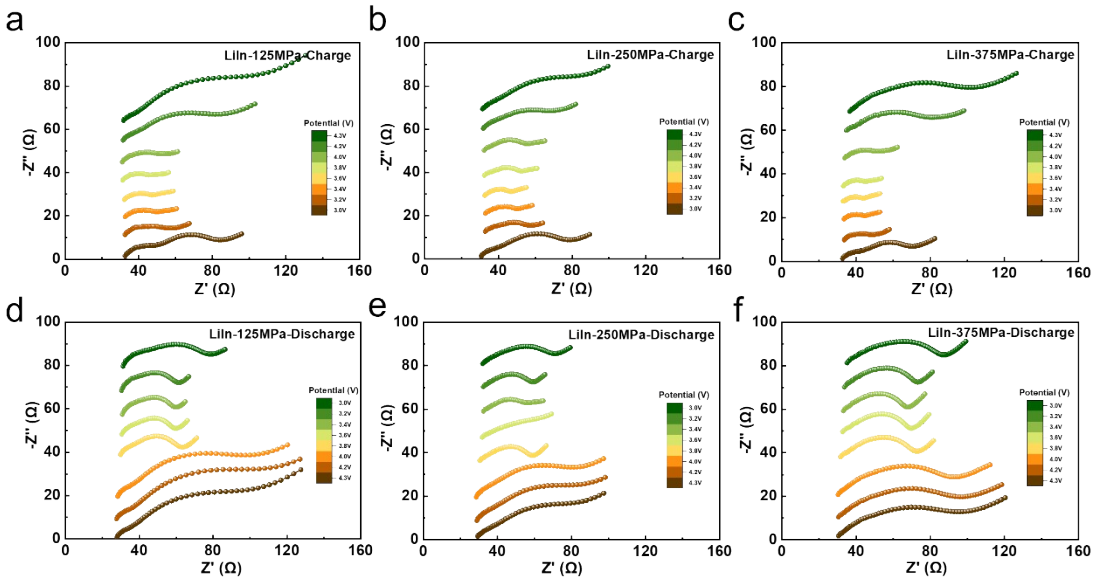

Figure S15. (a-c) In-situ EIS profiles during the first charging of LiIn-125MPa, LiIn-250MPa, and LiIn-375MPa between 3.0 and 4.3 V vs. Li/Li^+ at a 0.1C rate. (d-f) In-situ EIS profiles during the first discharging of LiIn-125MPa, LiIn-250MPa, and LiIn-375MPa between 3.0 and 4.3 V vs. Li/Li^+ at a 0.1C rate.

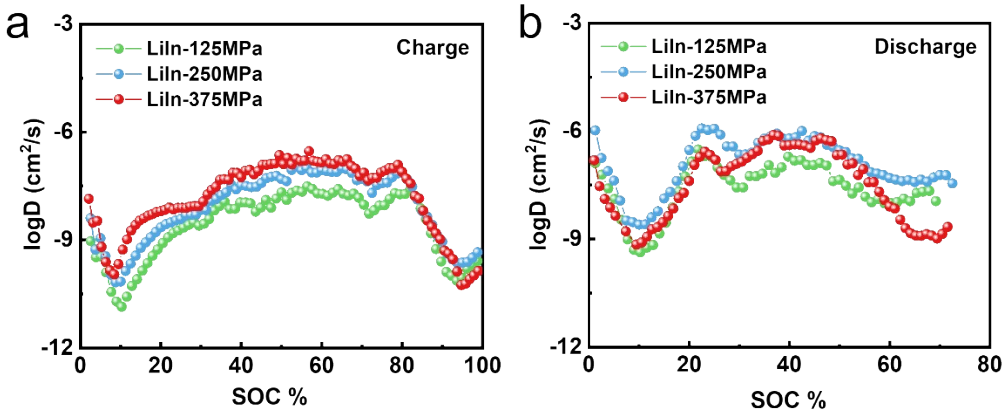

Figure S16. Diffusion coefficient for lithium ions computed from GITT curve as function of SOC during the first (a) charge and (b) discharge.

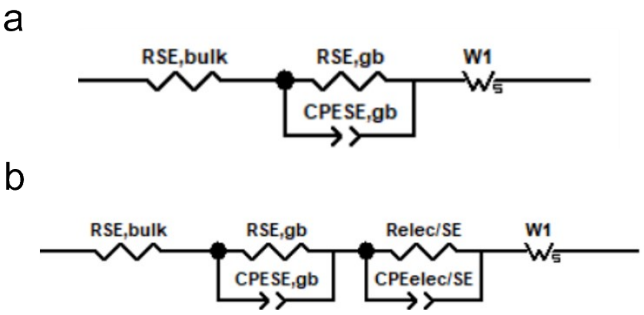

Figure S17. (a) The equivalent circuit diagram for EIS fitting without interfacial impedance. (b) The equivalent circuit diagram for EIS fitting with interfacial impedance.

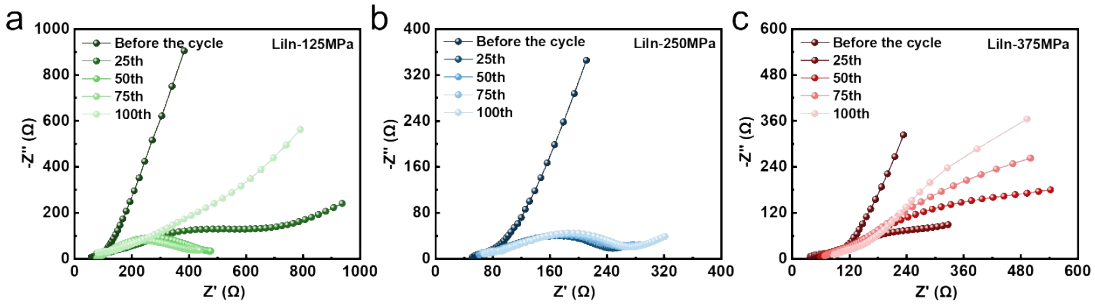

Figure S18. EIS variation during the cycling of (a) LiIn-125MPa, (b) LiIn-250MPa, and (c) LiIn-375MPa.

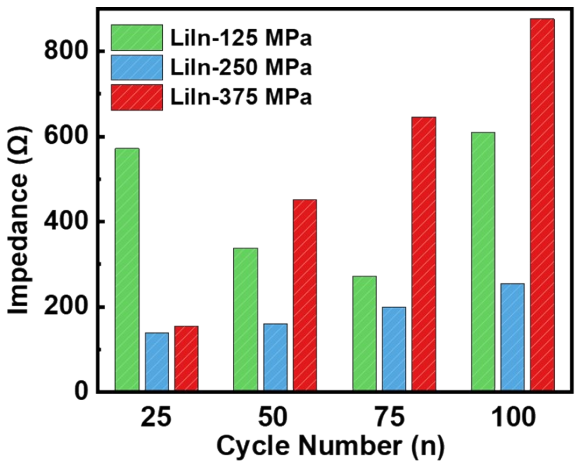

Figure S19. Impedance values of different NCM95s obtained from the fitted EIS during the cycling at 0.5C under different stacking pressure.

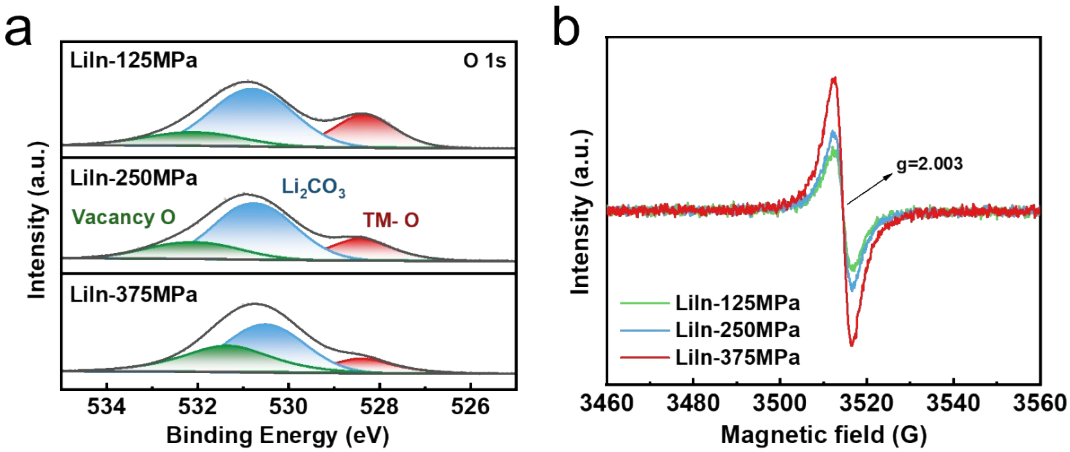

Figure S20. (a) The XPS spectra of O 1s and (b) EPR for the composite cathode after 200 cycles under different stacking pressure.

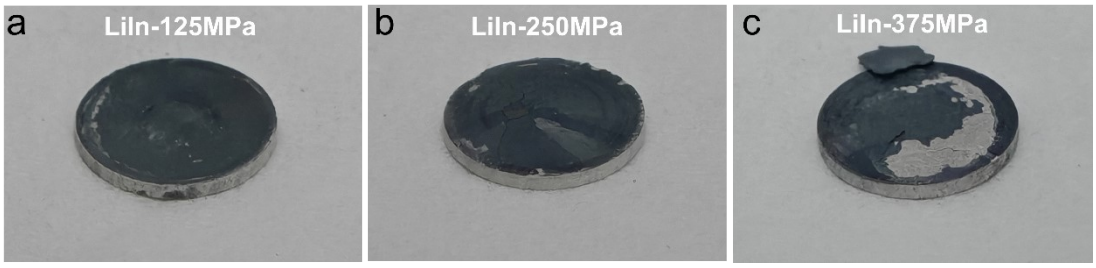

Figure S21. Optical photos of the electrode sheet of (a) LiIn-125MPa, (b) LiIn-250MPa, and (c) LiIn-375MPa. after 200 cycles.

Table S1 Interfacial impedance of each sample during the cycling. (Unit: Ω)

Sample	25^{th}	50^{th}	75^{th}	100^{th}
LiIn-125MPa	571.72	338.56	271.97	609.02
LiIn-250MPa	139.40	161.23	199.72	254.93
LiIn-375MPa	155.81	451.15	654.93	876.06

Table S2 The percentages of various groups identified from the S 2p after first charging and discharging under different stacking pressure. (Unit: %)

Sample	PS_4^{3-}	P_2S_x
LiIn-125MPa	82.5	17.5
LiIn-250MPa	74.8	25.2
LiIn-375MPa	70.2	29.8

Table S3 The percentages of various groups identified from the S 2p after 200 cycles under different stacking pressure. (Unit: %)

Sample	PS_4^{3-}	P_2S_x	SO_x
LiIn-125MPa	78.3	18.1	3.6
LiIn-250MPa	59.8	32.1	8.1
LiIn-375MPa	45.9	39.9	14.2